Release of tephra-hosted iron during early diagenesis fingerprinted by iron isotopes

Jack Longman[1*†], Ann G. Dunlea[2], Philipp Böning[1], Martin R. Palmer[3], Thomas M. Gernon[3], James McManus[4], Hayley R. Manners[5], William B. Homoky[6], Katharina Pahnke[1]

[1]Marine Isotope Geochemistry, Institute for Chemistry and Biology of the Marine Environment (ICBM), University of Oldenburg, Oldenburg, Germany

[2]Woods Hole Oceanographic Institution, Woods Hole, MA, USA.

[3]School of Ocean and Earth Sciences, University of Southampton, Southampton, UK

[4]Bigelow Laboratory for Ocean Sciences, East Boothbay, ME, USA.

[5]School of Geography, Earth and Environmental Sciences, University of Plymouth, Plymouth, UK.

[6]School of Earth and Environment, University of Leeds, Leeds, UK

[*]Corresponding author: jack2.longman@northumbria.ac.uk

[†] Present address: Department of Geography and Environmental Sciences, Northumbria University, Newcastle-upon-Tyne, UK

Abstract

The micronutrient iron (Fe) plays a fundamental role controlling primary productivity in the upper ocean, with volcanic eruptions and deposition of airborne volcanic material (termed tephra) a potential source of Fe. Here, we investigate the geochemical and Fe isotopic (δ^{56}Fe) composition of tephra layers, sediments, and mixed tephra-sediment samples from the Integrated Ocean Drilling Program (IODP) Hole 1396C, located offshore the volcanically active island of Montserrat in the Lesser Antilles, Caribbean Sea. We find that buried tephras, which have experienced diagenesis, exhibit lighter δ^{56}Fe (relative to standard IRMM-524a) compositions (down to -0.26 ± 0.04‰, 2SD) than fresh tephra deposited in Montserrat (δ^{56}Fe = 0.02 ± 0.02‰, 2SD). Such negative values suggest that isotopically heavier Fe has been lost from the originally deposited material. Using multivariate statistical modelling and mass balance constraints, we identify the outward Fe flux (with calculated δ^{56}Fe of 0.21 ± 0.31‰, 2SD, n=12) during non-reductive dissolution of tephra as the likely cause of the retention of these light δ^{56}Fe compositions. Due to the widespread nature of tephra deposition, tephra diagenesis may provide an important source of isotopically heavy dissolved Fe (dFe) to the oceans. This process contrasts with more commonly considered reductive dissolution processes, which provide a source of dFe enriched in light isotopes to the oceans.

1. Introduction

As an essential micronutrient for phytoplankton photosynthesis, dissolved iron (dFe) Fe)availability is directly linked to primary productivity and plankton community structure in modern high-latitude oceans (Falkowski et al., 1998; Kolber et al., 1994; Martin and Fitzwater, 1988; Tagliabue et al., 2017). Because primary productivity is one of the most important mechanisms determining air-sea CO_2 exchange, understanding Fe biogeochemistry is key to understanding marine carbon cycling (Tagliabue et al., 2017).

Dissolved (<0.2 µm) and particulate (>0.2µm) Fe is supplied to the ocean via rivers, aeolian deposition, hydrothermal vents and remobilization of sediment-hosted Fe (Homoky et al., 2013; Johnson et al., 2020; König et al., 2021). In addition, volcanism, and especially the eruptive dispersal of tephra, may provide an important episodic input of particulate Fe (pFe) to the Earth's surface environment (Longman et al., 2022; Olgun et al., 2011). Explosive volcanism results in the total eruption of ~1 km^3 of tephra (or unconsolidated pyroclastic material including pore space) every year (Pyle, 1995), and because most volcanoes are located on islands or near continental margins, as much as 45% of this tephra enters the ocean (Longman et al., 2022). Upon entering the ocean, tephra reacts rapidly with seawater, releasing of macro- and micro-nutrients such as dFe (Frogner et al., 2001; Jones and Gislason, 2008). A first estimate of the scale of this nutrient supply indicates tephra may deliver between 50 – 500 Gmol yr^{-1} of dFe to the oceans, with a median value of 180 Gmol yr^{-1} (Longman et al., 2022). The dFe delivery associated with tephra could therefore alleviate nutrient deficiencies for phytoplankton in Fe-limited regions of the ocean (Achterberg et al., 2013; Duggen et al., 2010; Moore et al., 2013; Olgun et al., 2013). Further, the release of other micronutrients such as dissolved Mn during this process mean tephra may also supply other co-limiting nutrients (Browning et al., 2021, 2014; Longman et al., 2020). The magnitude of this dFe source is also highlighted by the observation that roughly 30% of Pacific sediment located close to (i.e., within 1000km) of active arcs is comprised of tephra (Scudder et al., 2014, 2009). While the potential importance of tephra for oceanic Fe budgets is clear, the release of dFe during the diagenetic alteration of this volcanic material is poorly constrained and not yet represented

in the Fe-cycle parameterisation of any global ocean biogeochemical models (König et al., 2021; Tagliabue et al., 2016).

One method for investigating the cycling of Fe in the ocean uses its isotopic composition, typically presented as δ^{56}Fe relative to a measured standard. This composition can help trace the sources, sinks and cycling of Fe between the oceans and sediments (Conway and John, 2014; Homoky et al., 2013; Radic et al., 2011), provided the external sources of dFe and pFe to the oceans and the processes that fractionate Fe isotopes within and between them are understood (Johnson et al., 2020).

Typically, sources of dFe to the ocean such as dust and dFe released from oxic sediment, have isotopic signatures close to crustal values (0.09 ± 0.07‰; Beard et al., 2003). However, these compositions may be modified in parts of the ocean influenced by variable redox conditions (Johnson et al., 2020). For example, in low-oxygen sedimentary environments, reductive dissolution of Fe (a product of dissimilatory microbial reactions) leads to the release of dFe to porewaters with negative δ^{56}Fe compositions, with values reaching as low as -3.3‰ (Homoky et al., 2009). Hydrothermal vent fluids typically have δ^{56}Fe between -0.1 to -0.5‰ (Bennett et al., 2009; Johnson et al., 2020), but can be modified by the precipitation of sulfides or oxides. These precipitation reactions occur when either of the species are saturated in the fluids, and authigenic precipitates preferentially incorporate lighter isotopes when sulfides form and heavier isotopes when oxides form, thereby fractionating the remnant dFe in the fluid (Lough et al., 2017).

In addition to these reductive dissolution pathways, heavy (δ^{56}Fe > 0‰) lithogenic Fe signatures have been observed in porewaters (Homoky et al., 2021, 2013, 2009) and seawater (Conway and John, 2014; Radic et al., 2011) in some deep water locations. These heavy dFe values have been attributed to non-reductive dissolution (NRD) of lithogenic material in oxidising sediments, and indicates these oxic sediments may be an additional source of dFe to the oceans (Abadie et al., 2017; Homoky et al., 2013; König et al., 2021). This process, via the production of organo-mineral Fe colloids <0.2 µm in size, may provide a mechanism by which lithogenic δ^{56}Fe compositions are added to the ocean interior from oxidising margins (Homoky et al., 2021). Notably, the oxidative weathering of volcanoclastic marine sediments containing organic carbon between 0.3 – 0.6 % has produced the highest porewater

concentrations of dFe with crustal isotope compositions observed so far (Homoky et al., 2021), indicating these volcanogenic sediments could provide a uniquely important source of dFe for the ocean.

Here, we present Fe isotopic compositions from sediments, tephras and mixed sediment-tephra layers from offshore Montserrat in the Caribbean Sea to estimate the Fe isotopic composition of Fe lost during tephra transport and diagenesis. We combine these data with multivariate partitioning methods and calculations of the depletion factors and mass balance calculations to estimate the isotopic composition of Fe supplied to the ocean via dissolution of tephra during water column transport and early diagenesis.

2. Material and Methods

2.1. Study Site, Sampling and Age Model

Integrated Ocean Drilling Program (IODP) Hole 1396C was drilled as part of Expedition 340 in August-September 2012 (Le Friant et al., 2013). It is located ~30 km west of Montserrat at 16°30.5′N, 62°27.1′W (Fig. 1), and was drilled to a depth of 139.4 m below seafloor (mbsf). The core is carbonate-dominated, with abundant tephra layers and a minor contribution from terrigenous sediments. Bulk marine sediment and visually distinct discrete tephra layers were both sampled. For the samples from the tephra layers, efforts were made to sample from the centre of the layer to attain a purely volcanic signal. In addition to the IODP samples, we also studied fresh tephra from the 8th January 2010 eruption of the Soufrière Hills volcano, Montserrat.

2.2. Elemental analysis

Freeze-dried and homogenized tephra (n = 18) and sediment (n = 44) samples were dissolved using a mixed acid (HCl-HF-HNO_3) benchtop method. Solutions were diluted 1:5000 and analysed using a Thermo X-Series at the University of Southampton following the protocol of Longman et al. (2022). The certified reference material HISS-1 (sandy marine sediment), and procedural blanks were prepared and analysed in the same manner. For this work, a full suite of major and trace elements was analysed. Blank content was shown to be negligible for all elements, and recoveries for HISS-1 were within 10%

of expected values for most elements (see Supplementary Table 1). For Fe, two measurements of HISS-1 marine sediment standard averaged 2950 ppm, with an expected value of 2460 (recovery 97%). Blanks for Fe were on average 0.66 ppm, or 0.02% of the standard material. Porewater analysis of Fe was completed using the method of Murray et al. (2016). Briefly, pore waters were diluted to a 1:20 ratio using 1% distilled nitric acid before analysis on a Leeman Labs Prodigy ICP-OES at Oregon State University. The fresh tephra was analysed via X-Ray Fluorescence (Panalytical Axios Max) analysis at the University of Oldenburg. 700mg of sample was mixed with 4200 mg of Li-tetraborate, pre-oxidised at 500 °C with NH_4NO_3 and fused to form a glass bead. The in-house standard PS-S was prepared an analysed in the same manner. Fe_2O_3 content in the measured standard was 4.72%, compared to a long-term average of 4.76%, with repeat measurements within 0.1% of each other (n=3). In addition to the in-house standard, three certified reference materials (BE-N, JB-2 and SDO1) were prepared and analysed, with measured values of Fe_2O_3 close to certified values (see Supplementary Table 2).

2.3. Carbon analyses

Total organic carbon (TOC) measurements were made at Oregon State University following the method of Goñi et al. (2003), as reported in Murray et al. (2016). Further details on methods, blanks and reproducibility can be found in Murray et al. (2016).

2.4. Fe isotope analysis

A portion of the samples analysed for major and trace elements, and the fresh tephra samples, were analysed for their Fe isotope composition (n = 20). Samples were homogenized using an agate pestle and mortar prior to digestion of around 25 mg of sample via a mixed acid (HNO_3-$HClO_4$-HF) closed-vessel approach (Böning et al., 2004). Blanks and certified reference materials were dissolved in the same manner as samples. Aliquots of the digested samples were then purified via column chemistry (Böning et al., 2020; Dauphas et al., 2009). Samples were taken up in 6M HCl and Fe separation was performed using 1.8 mL AG1X8 anion resin (100–200 mesh, Bio-Rad) loaded onto PP columns (Bio-Rad). After separation, samples were treated with H_2O_2 to remove any organic compounds leached from

the columns, before drying. All purification was completed using ultra-clean acids in the clean laboratory facilities of the ICBM, University of Oldenburg.

Purified samples were diluted (to 3% HNO_3 and 3.3 ppm Fe) and analysed using a Thermo-Scientific Neptune *Plus* multi-collector inductively coupled plasma mass spectrometer (MC-ICP-MS) at the ICBM, Oldenburg. NIST 986 (National Institute of Standards and Technology, USA), a certified Ni isotope standard, was quantitatively added to each sample and standard for mass bias correction of up to 0.1 ‰ (Oeser et al., 2014). Signal intensity was ~15V for Fe and ~3V for Ni. Interference of ^{54}Cr on ^{54}Fe was monitored and corrected using ^{52}Cr (Weyer and Schwieters, 2003). Analysis of each sample was bracketed by a repeat standard (IRMM-524a), which is indistinguishable (within experimental uncertainty) from the more widely used isotope standard IRMM-14 (González De Vega et al., 2020). All results and comparisons to the literature are reported in delta notation relative to the mean of repeat IRMM-524 values (n = 112):

$$\delta^{56}Fe\ (‰) = [(^{56}Fe/^{54}Fe_{sample})/(^{56}Fe/^{54}Fe_{IRMM\text{-}524})] * 10^3$$

The reference materials SDO-1 (Devonian shale, US Geological Survey), BHVO-2 (Hawaiian basalt, US Geological Survey) and HISS-1 (marine sandy sediment, National Research Council of Canada) were used to assess the accuracy of Fe separations and measurements. Measurements of SDO-1 ($\delta^{56}Fe$ = 0.027 ± 0.017‰, n = 10, two digests, 2SD) were in good agreement with published values of 0.023 ± 0.028‰ (Schoenberg and Von Blanckenburg, 2005), and 0.026 ± 0.045‰ (Böning et al., 2020). Measurements of BHVO-2 ($\delta^{56}Fe$ = 0.078 ± 0.041‰, n = 3, 2SD) were within error of previously published values of 0.121 ± 0.049‰ (Liu et al., 2014), and 0.100 ± 0.060‰ (Foden et al., 2018). Procedural blanks were negligible (<0.1% of total Fe in the lowest concentration sample).

2.5. Numerical analysis

2.5.1. Multivariate Partitioning

We used a series of multivariate techniques to determine the sediment provenance and the relative contribution of each source to the sediment mixture deposited at Hole U1396C. First, we assessed the relationships between element concentrations with r^2 matrices, x versus y element plots, and ternary

plots to identify trends, outliers, and simple covariation patterns. Second, we selected elements in the dataset that were predominantly affiliated with the aluminosilicate fraction of the sediment and applied Q-mode Factor Analysis (QFA; Pisias et al., 2013). To ensure the robustness of the QFA results, we tested many combinations of elements, ran iterations with sample outliers removed, and assessed the sensitivity of the results when an additional factor was added or subtracted. Furthermore, we selected elements that were unique from those used in our tephra depletion model (Zr, Ti; see below) to determine if an independent technique produced similar results. Guided by the x versus y plots, ternary diagrams, and QFA results, elements and end-members were selected on the basis that they could be statistically differentiated in the dataset. The element concentration data were then modelled using constrained-least squares multiple linear regression (CLS; Pisias et al., 2013; Dunlea et al., 2015; Dunlea and Murray, 2015).

In the CLS mixing models, thousands of combinations of possible end-members from published studies or discrete layers measured in this study were tested to best fit the geochemical dataset in this study. The CLS model aims to minimize the difference between the model and measured data. Our preferred model was selected based on the strength of correlation coefficients of the CLS model and our geological knowledge of which sediment sources would feasibly be found at Hole U1396C (see Supplementary Tables 6-10; Supplementary Text).

2.5.2. Tephra Fe depletion calculations

We used two approaches to calculate early diagenetic Fe depletion factors for samples that were tephra-rich (>75% tephra contribution as estimated from the CLS model): Zr-normalization after Lee et al. (2018), and a multivariate CLS model. Zr-normalization compares the Fe/Zr and Ti/Zr ratios of the analysed ashes to a reference dataset of Caribbean volcanic rocks, derived from the GeoROC database (c.f. Longman et al., 2021; Longman et al., 2022). Data were downloaded from https://georoc.eu/, with all original publications and the specific search terms listed in the Supplementary Text. Here, Zr and Zr/Ti are assumed to be immobile whereas Fe may be mobilised during early diagenesis (Lee et al., 2018). The linear regression between the Fe/Zr and Ti/Zr of the igneous rock dataset is interpreted to represent the unaltered protolith of the tephra analysed here (Supplementary Figure 1). Using this

relationship and the measured Ti/Zr of the tephra layers, an original Fe/Zr composition can be back calculated, and depletion factors (DF) estimated, using the following equation:

$$DF_{Fe} = \frac{M_{Fe}^{L}}{M_{Fe}^{O}} = 1 - \frac{\left(\frac{C_{Fe}^{re}}{C_{Zr}^{re}}\right)}{\left(\frac{C_{Fe}^{O}}{C_{Zr}^{O}}\right)} \text{ (Eq. 1)}$$

Where the left side of the equation is the Fe depletion factor, DF_{Fe} (in %), with M_{Fe}^{O} the original Fe mass in the protolith and with M_{Fe}^{L} the mass of Fe lost from the protolith C_{Fe}^{re} and C_{Zr}^{re} are the mass concentrations of Fe and Zr in analysed tephra, and C_{Fe}^{O}/C_{Zr}^{O} represents the Fe/Zr ratio of the protolith. All masses are in wt%, with oxide content corrected where necessary.

A second approach, based on the end-member compositions and mass fractions from the CLS model was also applied to the discrete tephra layer and bulk sediment samples. The mass fraction of each end-member within each sample was multiplied by the concentration of Fe in that end-member. Summing the contributions of Fe from each end-member provides an estimate of how much Fe is expected in each sample if no Fe had been lost from the original tephra composition. As such, the total measured Fe in the sample can be subtracted from the predicted Fe content to obtain a depleted fraction:

$$f_{EM1}*[Fe]_{EM1} + f_{EM2}*[Fe]_{EM2} + f_{EM3}*[Fe]_{EM3} = \text{Total } [Fe]_{tephra} \text{ (Eq. 2)}$$

where f_{EM} = the fraction (0-1) of an end-member present in tephra. The difference between the predicted total Fe concentration in tephra (Total $[Fe]_{tephra}$) and the independently measured Fe content in tephra and sediment samples provides an estimate of the total Fe (wt. %) lost or gained during early diagenesis.

3. Results and Discussion

3.1. Sources of sediment in Hole U1396C

The multivariate statistical analyses identified three end-members defined from the major and trace metal dataset in the aluminosilicate fraction (i.e., non-carbonate component) of sediment at Hole U1396C. Because the Al and Ti concentrations are much higher than the concentrations of the other trace elements, they have more influence on the outcome of the model. For example, the magnitude of

a small variation in Al can still be much larger than a relatively significant variation in Nb. To avoid this bias toward higher concentration elements, we did not use Al and Ti in the CLS model and instead relied on elements in the ppm range. The factor analysis suggests that three aluminosilicate components can be distinguished with or without Al and Ti included. In our preferred model, the QFA uses a combination of trace and rare earth elements (Co, Nb, Y, La, Ce, Eu, Yb, and Th) to explain 97% of the data variability with three factors (Fig. 2). The first aluminosilicate factor identified in the QFA explained 45% of the variability in the dataset and indicated a strong covariance (i.e., high VARIMAX factor scores) among Nb, La, Ce, and Th throughout the samples (Fig. 2). The second factor explained 36% of the variability of the dataset and indicated a strong covariance among Y, Ce, Eu, and Yb. The third factor explained 16% of the dataset and showed a covariance between Co and Eu.

After testing thousands of different combinations of end-members in the CLS model to find the best fit for these element concentrations (Dunlea and Murray, 2015), QFA Factors 1 – 3 were interpreted to represent a continental dust source and two andesitic tephra end-members, respectively. In the CLS model, a continental dust end-member was chosen to approximate the composition of upper continental crust (Rudnick and Gao, 2013). This interpretation is in accord with previous studies that show Saharan dust forms a minor component of marine sediments in this area (Reid et al., 1996). The first andesitic tephra with a more felsic composition used in the model was a discrete tephra layer measured in this study (134.63 mbsf at Site U1396), but was also represented well by a subaerial tephra from Montserrat (Sample 11.1.4C from Coussens et al., 2017). The second andesitic tephra end-member with a more mafic composition than the other andesitic tephra layers is represented best by a tephra composition from the Las Sierra volcanoes in Nicaragua (Schindlbeck et al., 2018), but the composition is also similar to a subaerial tephra from Monserrat (Sample 9.2.1E from Coussens et al., 2017). Based on its proximity, subaerial tephra from Montserrat was selected as the more likely for Site U1396C (Fig. 3).

Previous work offshore Montserrat has indicated that sediments are a three-component mixture (terrestrial, $CaCO_3$ and tephra) and that Cr depletion can be used as a proxy for tephra content (Peters et al., 2000; Scudder et al., 2016). Our approach builds on this normative calculation, as it considers a range of elements. Our findings support previous work that indicates much of the tephra in marine

sediments is not in discrete layers, but is in the 'dispersed' tephra component (Peters et al., 2000; Scudder et al., 2009; 2014). That is, tephra that has undergone some form of mixing process (e.g. bioturbation, transport in the water column) is not visible in sediment cores as discrete layers (Scudder et al., 2009; 2016). As expected, with 'tephra layers' (identified as layers with $CaCO_3$ <10 wt.%), the tephra component is typically >85 wt.% (89 ± 13 wt.%, 1SD, n = 18). However, in the bulk sediment samples, the combined andesite tephra (i.e., the dispersed tephra component) contribution remains high (29 ± 10 wt.%, 1 SD, n = 43), with a maximum of 55 wt.% (Fig. 3). An average of 29 wt.% is higher than the previous upper estimate of dispersed tephra in this region's sediment (between 15 – 20 wt.%; Peters et al., 2000), and confirms the importance of tephra deposition in Caribbean sediments.

3.2. Fe isotope systematics

The δ^{56}Fe values in tephra-rich samples from U1396C range from -0.26 to 0.01 ‰, with an average of -0.12 ± 0.08 ‰ (1SD, n = 19). 18 of 19 samples fall outside of the range of crustal rocks (0.09 ± 0.07 ‰, as defined by Beard et al. 2003), and none have a δ^{56}Fe composition higher than these crustal rocks (Fig. 4; Supplementary Table 3). Our measured Fe isotope value of terrestrial tephra on Montserrat (δ^{56}Fe = -0.019 ± 0.02‰) is within the envelope of crustal rock compositions, and similar to previous measurements of volcanics from the Lesser Antilles , which yielded a δ^{56}Fe value of 0.045 ± 0.039‰ (Foden et al., 2018). These measurements on the Lesser Antilles volcanics were completed on lava samples from onshore outcrops, and so the comparability between the two values suggests little Fe isotope fractionation occurs during the eruption of explosive volcanic products in the Lesser Antilles arc. While airborne transport may alter Fe speciation (Maters et al., 2017) and total Fe content of the tephra (Simonella et al., 2015), atmospheric processes do not significantly alter the Fe isotope composition of the tephra.

Measurements of marine sediment and tephra samples from Hole U1396C, show considerable variation from what may be considered a magmatic rock Fe isotope composition, with subaerial volcanic rock isotope compositions typically between −0.054 and 0.1 ‰ (Foden et al., 2018; Johnson et al., 2020). Thus, our data indicate that some process within the tephra-rich sediments leads to more negative δ^{56}Fe values in the tephras recovered from marine sediments than observed in subaerial volcanic rocks. This

process may involve a diagenetic reaction, admixture of other sedimentary sources with distinct Fe isotopic compositions, and/or interaction with dFe from seawater.

To investigate the possibility that the total isotopic composition ($\delta^{56}Fe_{Total}$) reflects the mixture of tephra with terrigenous and carbonate contributions, we assume the isotopic composition is governed by the mass-balance of these sources ($\delta^{56}Fe_{ash}$, $\delta^{56}Fe_{terr}$ and $\delta^{56}Fe_{carb}$, respectively; Eq. 3):

$$\delta^{56}Fe_{Total} = (\delta^{56}Fe_{Tephra} \times f_{Tephra}) + (\delta^{56}Fe_{terr} \times f_{terr}) + (\delta^{56}Fe_{Carb} \times f_{carb}) \text{ (Eq. 3)}$$

Where f is the molar fraction of each component. However, there is no evidence for any Fe-rich carbonates (such as siderite) in the Caribbean Sea, and only aragonite and Mg-rich carbonate have been reported (Reid et al., 1996), hence this fraction is likely to contain low levels of Fe (Fe/Ca of below 30 $\mu mol\ mol^{-1}$; see Boyle, 1981). Any Fe associated with the biogenic carbonate will be present only in the form of Fe-Mn diagenetic coatings (Boyle, 1981). Further, chemical extractions used to detect the presence of Fe-carbonates in marine sediments adjacent to Montserrat also confirmed at most only trace abundances (<0.02 dwt % of total sediment or <0.5 dwt% of total Fe; Homoky et al., 2011). As such, we consider the carbonate contribution to the isotopic mixture to be negligible, and so simplify the equation as follows (Eq. 4):

$$\delta^{56}Fe_{Total} = (\delta^{56}Fe_{Tephra} \times f_{Tephra}) + (\delta^{56}Fe_{terr} \times f_{terr}) \text{ (Eq. 4)}$$

We can use our measured estimate of $\delta^{56}Fe$ for terrestrial tephra (-0.019 ± 0.023 ‰; $\delta^{56}Fe_{Tephra}$), published estimates of the $\delta^{56}Fe$ of terrigenous material (c. 0.01 ± 0.05 ‰; $\delta^{56}Fe_{Terr}$, Beard et al., 2003), and the proportion estimates for tephra (combining the contribution of the two andesites) and terrigenous material (f_{Ash}, f_{Terr}) from the CLS model to assess if a simple mixture may explain the measured Fe composition in our samples. Using the values of $\delta^{56}Fe_{Tephra}$ and $\delta^{56}Fe_{Terr}$ and the error defined above, the most negative $\delta^{56}Fe$ composition produced by these mixtures is -0.043‰ (significantly more positive than most of the samples measured from U1396C).

One of the key diagenetic processes that acts on tephra in marine sediment is dissolution and leaching (Jones and Gislason, 2008; Longman et al., 2019). Here, we focus on those 12 samples containing >75 wt.% ash (the closest representatives of ‘pure’ tephra samples within our sample suite) to test whether

diagenesis favours the loss of heavy Fe isotopes and the retention of isotopically light (δ^{56}Fe lower than -0.1‰) Fe in the sediment. In this mass balance calculation, we assume that the measured δ^{56}Fe ($\delta^{56}Fe_{Measured}$) is the result of the modification of the original tephra, with the dFe lost through early diagenesis represented by the proportion f_{Lost}. In this scenario, the $\delta^{56}Fe_{Measured}$ comprises the following mass balance (Eq. 5):

$$\delta^{56}Fe_{Measured} = (\delta^{56}Fe_{Tephra} \times f_{Tephra}) - (\delta^{56}Fe_{Lost} \times f_{Lost}) \text{ (Eq. 5)}$$

The calculated $\delta^{56}Fe_{Lost}$ values, are considered representative of the isotopic composition of the Fe lost during early diagenesis, and f_{Lost} is the proportion of Fe that was lost from the protolith. f_{Lost} can be estimated using depletion factor (DF_{Fe}) calculations (see Methods and Materials), which estimate how much Fe has been lost. Firstly via a Zr depletion model as detailed in Lee et al. (2018), and secondly via a CLS-based model, using outputs from the multivariate partitioning. Therefore, f_{Tephra} is calculated by subtracting f_{Lost} from 1. By rearranging equation 5, and using these independent DF_{Fe} estimates as f_{Lost}, we can solve for $\delta^{56}Fe_{Lost}$ as follows:

$$\delta^{56}Fe_{Lost} = (\delta^{56}Fe_{ash} \times f_{Tephra}) - (\delta^{56}Fe_{Measured})/f_{Lost} \text{ (Eq. 6)}$$

As we use two methods to estimate DF_{Fe}, we derive two estimates for $\delta^{56}Fe_{Lost}$ (see Fig. 5), but they are in good agreement (Supplementary Figure 2), with significant correlation between the two ($r^2 = 0.65$, p-value 0.02, n = 12). Although the estimated ranges of f_{Lost} vary between our DF_{Fe} methods (Zr normalization model-12 to 80%, CLS Model -3 to 54%,), both approaches yield similar results and suggest net positive values for $\delta^{56}Fe_{Lost}$ relative to the original isotopic composition of the tephra. A single sample appears to have gained Fe through diagenesis, potentially through reprecipitation of Fe-bearing phases, reflected in the negative model result (Fig. 5). The results derived from Zr-normalization show slightly higher mean values for $\delta^{56}Fe_{Lost}$ (0.36 ± 0.28‰, 1SD, n = 12) within uncertainty of the mean value derived from our CLS modelling approach (0.21 ± 0.15‰, 1SD, n=12). These positive values for δ^{56}Fe are similar to measurements of dFe supplied to porewater and seawater via non-reductive dissolution (NRD), as inferred in oxidizing pore water δ^{56}Fe from tephra-rich sediments near the Crozet Islands (0.16 ± 0.05‰; Homoky et al., 2009), the Cape Margin (0.22‰; Homoky et al.,

2013), western South Atlantic ($\delta^{56}Fe = 0.07 \pm 0.07‰$; Homoky et al., 2021) and New Guinea Coastal waters (0.37 ± 0.15‰; Radic et al., 2011).

It is assumed that NRD does not derive from a chemical reaction specifically for Fe — rather the release of Fe following the physical and chemical weathering of primary host-silicate structures – a process that by itself should not fractionate Fe isotopes. However, the chelation of ferric ions by organic ligands is known to favour heavier Fe isotopes, with fractionation factors of between +0.2 to +0.5‰ observed experimentally (Dideriksen et al., 2008; Morgan et al., 2010), and in the natural environment (Ilina et al., 2013). Ligand-complexation is also used to explain dissolved $\delta^{56}Fe$ values in North Atlantic surface waters that are +0.2 to +0.6‰ higher than the pFe source in Saharan dust (Conway and John, 2014). The fractionation effect attributed to NRD of pFe elsewhere in the ocean interior is shown to be on average +0.2‰ enriched in the dissolved pool (Radic et al.,2011; Labatut et al., 2014; Abadie et al., 2017). Therefore, it is likely the isotopic fractionation of f_{Lost} observed in our analysis represents the primary signature from NRD of tephra, and any physicochemical transformations to more stable dissolved phases. These transformations may involve ferric ion chelation by organic ligands, and/or the precipitation and stabilisation of colloidal Fe (oxyhydr)oxides with organic carbon. Collectively, the non-reductive formation of these dissolved Fe species will favour the mobilisation and net loss of heavier Fe isotopes from the sediment protolith. Previous studies have shown that NRD may only result in small benthic Fe fluxes in some settings (Homoky et al., 2013), but fluxes out of the sediment may be enhanced in locations of high volcanogenic (Homoky et al., 2011) and lithogenic (e.g. dust, riverine particles) deposition and/or sediment re-suspension (Homoky et al., 2021; Klar et al., 2018; Labatut et al., 2014; Lam et al., 2020).

The regular and large-scale input of tephra from volcanoes in Central America (e.g. Schindlbeck et al., 2016), and the Lesser Antilles (Coussens et al., 2017; Palmer et al., 2016) provides a significant source of volcanic material for the Caribbean Sea. In a similar manner to western Africa, where input of lithogenic material via riverine input leads to a large supply of Fe from NRD (Klar et al., 2018), our data suggest the deposition of tephra in the Caribbean may act as a source of Fe to seawater, via NRD. Indeed, tephra is known to rapidly release Fe via interactions with seawater (Jones and Gislason, 2008),

and during early diagenesis (Longman et al., 2022, 2019). This release from tephra is inferred from the relatively high Fe content in pore waters from U1396C (typical values between 10 – 50 μmol; Fig. 2), and dissolution of tephra is also reflected in the volcanogenic Sr isotope composition of the pore waters (Fig. 4; Murray et al., 2018).

Further evidence for the non-reductive release of dFe from tephra in the marine sediments comes from young tephra deposited in the Caribbean Sea and Holocene-aged volcanogenic turbidites deposited around the Crozet Islands, Southern Ocean. An 18-month old tephra deposit sampled in deep-water off Montserrat revealed the efficient consumption of pore water oxygen and high levels of dFe and dMn (micro-molar concentrations) accumulated in pore waters in the absence of organic carbon to drive bacterial metal reduction (Homoky et al., 2011). Hembury et al. (2012) attributed this oxygen consumption in the tephra to reaction with inorganic minerals, consistent with the idea that high pore water dFe and dMn contents resulted from the NRD of tephra in seawater rather than bacterial dissimilatory reduction. Analogous, but Holocene-aged, volcanogenic turbidites around the Crozet Islands also display micro-molar levels of dFe and dMn in pore waters, here present as colloids in the presence of oxygen. A non-reductive provenance of dFe in pore water (and likely ligand binding) was also confirmed by its δ^{56}Fe values between -0.01 and 0.12‰ (Homoky et al., 2011, 2009). Evidently, we can expect to see comparative differences in the physical chemistry of dFe within marine sediments due to variations in sediment and seawater admixtures and reaction times, but the primary, rapid and non-reductive release of Fe from volcanic tephra during transport through the water column and after deposition at the seafloor appears to be a defining characteristic of volcanic sedimentation elsewhere, consistent with our findings. Evidence for the impact of NRD on regional Fe budgets might be identified in δ^{56}Fe compositions of western North Atlantic seawater. For example, dissolved δ^{56}Fe values from 0.2 to 0.74‰ in seawater down to 4200 metres offshore Bermuda (Conway and John, 2014; John and Adkins, 2012), are within the range we have calculated as $\delta^{56}Fe_{Lost}$ (Fig. 5). Presently, these Fe isotope compositions are attributed to a mixture of dust fractionation and organic ligand-mediated processes (Conway and John, 2014; John and Adkins, 2012; König et al., 2021). We suggest that input of dFe from tephra-rich sediment alteration may also contribute to these isotopically heavy δ^{56}Fe values in the

Bermudan samples via the advection of benthic nepheloid layers that are thought to enter this region from the Caribbean and Gulf of Mexico (Feely, 1975; McCave, 1986), but additional new analyses of Caribbean Sea seawater may be needed to test this hypothesis.

4. Conclusions

We measured the major and trace element concentration and Fe isotopic composition of tephra and sediment layers from the Caribbean Sea. The bulk sediment is dominated by biogenic carbonate, but using a multivariate partitioning approach, we determined that aluminosilicate material in the sediment is a mixture of three primary sources, two linked to tephra deposition and one linked to terrestrial input. Overall, dispersed tephra comprises 29% of all sediment analyzed in this study. Fe isotope analyses indicate that tephra within the sediment, which has undergone water column transport and subsequent diagenesis, has δ^{56}Fe values that are isotopically lighter than its source material, with δ^{56}Fe values as low as -0.26‰. This value is considerably lighter than measured δ^{56}Fe from fresh tephra (which we show to be close to 0 ‰). Modelling of these Fe isotope data using multivariate partitioning suggests that the negative δ^{56}Fe values of sediment hosted tephra layers results from the preferential loss of heavy Fe isotopes during diagenesis of tephra. This Fe loss most likely occurs as the result of non-reductive dissolution of the silicate material and the mobilisation of tephra hosted Fe in a dissolved phase. We suggest this tephra dissolution may provide an important source of dissolved Fe and possibly other micro-nutrient elements for phytoplankton metabolism and marine biogeochemical cycles in the vicinity of volcanoes. Further, the deposition and dissolution of volcanic material might be traced by its influence on the mean isotope composition of dissolved Fe in seawater connected to regions of volcanic sedimentation.

Acknowledgements

This manuscript used samples provided by the Integrated Ocean Drilling Program (IODP) from Expedition 340. IODP is sponsored by the U.S. National Science Foundation (NSF). The authors are grateful to the co-chief scientists A. Le Friant and O. Ishizuka of Expedition 340 as well as all the participants in the expedition for their contributions to the sea-going effort. Appreciation is extended to

Jesse Muratli at Oregon State University for his work in the laboratory. Financial support was provided by the United States Science Support Program (USSSP) and the US National Science Foundation to JM under grant Numbers 1360077 and 1715106 for shore-based analyses. MRP and TG acknowledge NERC grant NE/K00543X/1.

References

Abadie, C., Lacan, F., Radic, A., Pradoux, C., Poitrasson, F., 2017. Iron isotopes reveal distinct dissolved iron sources and pathways in the intermediate versus deep Southern Ocean. Proc. Natl. Acad. Sci. U. S. A. 114, 858–863. https://doi.org/10.1073/pnas.1603107114

Achterberg, E.P., Moore, C.M., Henson, S.A., Steigenberger, S., Stohl, A., Eckhardt, S., Avendano, L.C., Cassidy, M., Hembury, D., Klar, J.K., Lucas, M.I., Macey, A.I., Marsay, C.M., Ryan-Keogh, T.J., 2013. Natural iron fertilization by the Eyjafjallajökull volcanic eruption. Geophys. Res. Lett. 40, 921–926. https://doi.org/10.1002/grl.50221

Beard, B.L., Johnson, C.M., Von Damm, K.L., Poulson, R.L., 2003. Iron isotope constraints on Fe cycling and mass balance in oxygenated Earth oceans. Geology 31, 629–632. https://doi.org/10.1130/0091-7613(2003)031<0629:IICOFC>2.0.CO;2

Bennett, S.A., Rouxel, O., Schmidt, K., Garbe-Schönberg, D., Statham, P.J., German, C.R., 2009. Iron isotope fractionation in a buoyant hydrothermal plume, 5°S Mid-Atlantic Ridge. Geochim. Cosmochim. Acta 73, 5619–5634. https://doi.org/10.1016/J.GCA.2009.06.027

Böning, P., Brumsack, H.J., Böttcher, M.E., Schnetger, B., Kriete, C., Kallmeyer, J., Borchers, S.L., 2004. Geochemistry of Peruvian near-surface sediments. Geochim. Cosmochim. Acta 68, 4429–4451. https://doi.org/10.1016/j.gca.2004.04.027

Böning, P., Schnetger, B., Belz, L., Ferdelman, T., Brumsack, H.J., Pahnke, K., 2020. Sedimentary iron cycling in the Benguela upwelling system off Namibia. Earth Planet. Sci. Lett. 538, 116212. https://doi.org/10.1016/J.EPSL.2020.116212

Boyle, E.A., 1981. Cadmium, zinc, copper, and barium in foraminifera tests. Earth Planet. Sci. Lett. 53, 11–35. https://doi.org/10.1016/0012-821X(81)90022-4

Browning, T.J., Achterberg, E.P., Engel, A., Mawji, E., 2021. Manganese co-limitation of phytoplankton growth and major nutrient drawdown in the Southern Ocean. Nat. Commun. 12, 1–9. https://doi.org/10.1038/s41467-021-21122-6

Browning, T.J., Bouman, H.A., Henderson, G.M., Mather, T.A., Pyle, D.M., Schlosser, C., Woodward, E.M.S., Moore, C.M., 2014. Strong responses of Southern Ocean phytoplankton communities to volcanic ash. Geophys. Res. Lett. 41, 2851–2857. https://doi.org/10.1002/2014GL059364

Conway, T.M., John, S.G., 2014. Quantification of dissolved iron sources to the North Atlantic Ocean. Nature 511, 212–215. https://doi.org/10.1038/nature13482

Coussens, M., Cassidy, M., Watt, S.F.L., Jutzeler, M., Talling, P.J., Barfod, D., Gernon, T.M., Taylor, R., Hatter, S.J., Palmer, M.R., 2017. Long-term changes in explosive and effusive behaviour at andesitic arc volcanoes: Chronostratigraphy of the Centre Hills Volcano, Montserrat. J. Volcanol. Geotherm. Res. 333–334, 15–35. https://doi.org/10.1016/j.jvolgeores.2017.01.003

Dauphas, N., Pourmand, A., Teng, F.Z., 2009. Routine isotopic analysis of iron by HR-MC-ICPMS: How precise and how accurate? Chem. Geol. 267, 175–184. https://doi.org/10.1016/J.CHEMGEO.2008.12.011

Dideriksen, K., Baker, J.A., Stipp, S.L.S., 2008. Equilibrium Fe isotope fractionation between inorganic aqueous Fe(III) and the siderophore complex, Fe(III)-desferrioxamine B. Earth Planet. Sci. Lett. 269, 280–290. https://doi.org/10.1016/J.EPSL.2008.02.022

Duggen, S., Olgun, N., Croot, P., Hoffmann, L., Dietze, H., Delmelle, P., Teschner, C., 2010. The role of airborne volcanic ash for the surface ocean biogeochemical iron-cycle: a review. Biogeosciences 7, 827–844. https://doi.org/10.5194/bg-7-827-2010

Dunlea, A.G., Murray, R.W., 2015. Optimization of end-members used in multiple linear regression geochemical mixing models. Geochemistry, Geophys. Geosystems 16, 4021–4027. https://doi.org/10.1002/2015GC006132

Dunlea, A.G., Murray, R.W., Sauvage, J., Spivack, A.J., Harris, R.N., D'Hondt, S., 2015. Dust, volcanic ash, and the evolution of the South Pacific Gyre through the Cenozoic. Paleoceanography 30, 1078–1099. https://doi.org/10.1002/2015PA002829

Falkowski, P.G., Barber, R.T., Smetacek, V., 1998. Biogeochemical controls and feedbacks on ocean primary production. Science (80-.). https://doi.org/10.1126/science.281.5374.200

Feely, R.A., 1975. Major-element composition of the particulate matter in the near-bottom nepheloid layer of the gulf of Mexico. Mar. Chem. 3, 121–156. https://doi.org/10.1016/0304-4203(75)90019-5

Foden, J., Sossi, P.A., Nebel, O., 2018. Controls on the iron isotopic composition of global arc magmas. Earth Planet. Sci. Lett. 494, 190–201. https://doi.org/10.1016/J.EPSL.2018.04.039

Frogner, P., Reynir Gíslason, S., Óskarsson, N., 2001. Fertilizing potential of volcanic ash in ocean surface water. Geology 29, 487. https://doi.org/10.1130/0091-7613(2001)029<0487:FPOVAI>2.0.CO;2

Goñi, M.A., Teixeira, M.J., Perkeya, D.W., 2003. Sources and distribution of organic matter in a river-dominated estuary (Winyah Bay, SC, USA). Estuar. Coast. Shelf Sci. 57, 1023–1048. https://doi.org/10.1016/S0272-7714(03)00008-8

González De Vega, C., Chernonozhkin, S.M., Grigoryan, R., Costas-Rodríguez, M., Vanhaecke, F., 2020. Characterization of the new isotopic reference materials IRMM-524A and ERM-AE143 for Fe and Mg isotopic analysis of geological and biological samples. J. Anal. At. Spectrom. 35, 2517–2529. https://doi.org/10.1039/D0JA00225A

Hembury, D.J., Palmer, M.R., Fones, G.R., Mills, R.A., Marsh, R., Jones, M.T., 2012. Uptake of dissolved oxygen during marine diagenesis of fresh volcanic material. Geochim. Cosmochim. Acta 84, 353–368. https://doi.org/10.1016/J.GCA.2012.01.017

Homoky, W.B., Conway, T.M., John, S.G., König, D., Deng, F.F., Tagliabue, A., Mills, R.A., 2021. Iron colloids dominate sedimentary supply to the ocean interior. Proc. Natl. Acad. Sci. U. S. A. 118. https://doi.org/10.1073/PNAS.2016078118

Homoky, W.B., Hembury, D.J., Hepburn, L.E., Mills, R.A., Statham, P.J., Fones, G.R., Palmer, M.R., 2011. Iron and manganese diagenesis in deep sea volcanogenic sediments and the origins of pore water colloids. Geochim. Cosmochim. Acta 75, 5032–5048. https://doi.org/10.1016/J.GCA.2011.06.019

Homoky, W.B., John, S.G., Conway, T.M., Mills, R.A., 2013. Distinct iron isotopic signatures and supply from marine sediment dissolution. Nat. Commun. 4, 1–10. https://doi.org/10.1038/ncomms3143

Homoky, W.B., Severmann, S., Mills, R.A., Statham, P.J., Fones, G.R., 2009. Pore-fluid Fe isotopes reflect the extent of benthic Fe redox recycling: Evidence from continental shelf and deep-sea sediments. Geology 37, 751–754. https://doi.org/10.1130/G25731A.1

Ilina, S.M., Poitrasson, F., Lapitskiy, S.A., Alekhin, Y. V., Viers, J., Pokrovsky, O.S., 2013. Extreme iron isotope fractionation between colloids and particles of boreal and temperate organic-rich waters. Geochim. Cosmochim. Acta 101, 96–111. https://doi.org/10.1016/J.GCA.2012.10.023

John, S.G., Adkins, J., 2012. The vertical distribution of iron stable isotopes in the North Atlantic near Bermuda. Global Biogeochem. Cycles 26, 2034. https://doi.org/10.1029/2011GB004043

Johnson, C., Beard, B., Weyer, S., 2020. Iron Geochemistry: An Isotopic Perspective.

Jones, M.T., Gislason, S.R., 2008. Rapid releases of metal salts and nutrients following the deposition of volcanic ash into aqueous environments. Geochim. Cosmochim. Acta 72, 3661–3680. https://doi.org/10.1016/j.gca.2008.05.030

Klar, J.K., Schlosser, C., Milton, J.A., Woodward, E.M.S., Lacan, F., Parkinson, I.J., Achterberg, E.P., James, R.H., 2018. Sources of dissolved iron to oxygen minimum zone waters on the Senegalese continental margin in the tropical North Atlantic Ocean: Insights from iron isotopes. Geochim. Cosmochim. Acta 236, 60–78. https://doi.org/10.1016/j.gca.2018.02.031

Kolber, Z.S., Barber, R.T., Coale, K.H., Fitzwateri, S.E., Greene, R.M., Johnson, K.S., Lindley, S., Falkowski, P.G., 1994. Iron limitation of phytoplankton photosynthesis in the equatorial Pacific Ocean. Nature 371, 145–149. https://doi.org/10.1038/371145a0

König, D., Conway, T.M., Ellwood, M.J., Homoky, W.B., Tagliabue, A., 2021. Constraints on the Cycling of Iron Isotopes From a Global Ocean Model. Global Biogeochem. Cycles 35, e2021GB006968. https://doi.org/10.1029/2021GB006968

Labatut, M., Lacan, F., Pradoux, C., Chmeleff, J., Radic, A., Murray, J.W., Poitrasson, F., Johansen, A.M., Thil, F., 2014. Iron sources and dissolved-particulate interactions in the seawater of the Western Equatorial Pacific, iron isotope perspectives. Global Biogeochem. Cycles 28, 1044–1065. https://doi.org/10.1002/2014GB004928

Lam, P.J., Heller, M.I., Lerner, P.E., Moffett, J.W., Buck, K.N., 2020. Unexpected Source and Transport of Iron from the Deep Peru Margin. ACS Earth Sp. Chem. 4, 977–992. https://doi.org/10.1021/ACSEARTHSPACECHEM.0C00066/ASSET/IMAGES/LARGE/SP0C00066_0009.JPEG

Le Friant, A., Ishizuka, O., Stroncik, N.A., Expedition 340 Scientists, T., 2013. Proc. IODP, 340. Integrated Ocean Drilling Program Management International, Inc., Tokyo.

Lee, C.-T.A., Jiang, H., Ronay, E., Minisini, D., Stiles, J., Neal, M., 2018. Volcanic ash as a driver of enhanced organic carbon burial in the Cretaceous. Sci. Rep. 8, 4197. https://doi.org/10.1038/s41598-018-22576-3

Liu, S.A., Teng, F.Z., Li, S., Wei, G.J., Ma, J.L., Li, D., 2014. Copper and iron isotope fractionation during weathering and pedogenesis: Insights from saprolite profiles. Geochim. Cosmochim. Acta 146, 59–75. https://doi.org/10.1016/J.GCA.2014.09.040

Longman, J., Mills, B.J.W., Manners, H.R., Gernon, T.M., Palmer, M.R., 2021. Late Ordovician climate change and extinctions driven by elevated volcanic nutrient supply. Nat. Geosci. 14, 924–929. https://doi.org/10.1038/s41561-021-00855-5

Longman, J., Palmer, M.R., Gernon, T.M., 2020. Viability of greenhouse gas removal via artificial addition of volcanic ash to the ocean. Anthropocene 32. https://doi.org/10.1016/j.ancene.2020.100264

Longman, J., Palmer, M.R., Gernon, T.M., Manners, H.R., 2019. The role of tephra in enhancing organic carbon preservation in marine sediments. Earth-Science Rev. 192, 480–490. https://doi.org/10.1016/j.earscirev.2019.03.018

Longman, J., Palmer, M.R., Gernon, T.M., Manners, H.R., Jones, M.T., 2022. Subaerial volcanism as

a major contributor to oceanic iron and manganese cycles. Commun. Earth Environ.

Lough, A.J.M., Klar, J.K., Homoky, W.B., Comer-Warner, S.A., Milton, J.A., Connelly, D.P., James, R.H., Mills, R.A., 2017. Opposing authigenic controls on the isotopic signature of dissolved iron in hydrothermal plumes. Geochim. Cosmochim. Acta 202, 1–20. https://doi.org/10.1016/J.GCA.2016.12.022

Martin, J.H., Fitzwater, S.E., 1988. Iron deficiency limits phytoplankton growth in the north-east pacific subarctic. Nature 331, 341–343. https://doi.org/10.1038/331341a0

Maters, E.C., Delmelle, P., Gunnlaugsson, H.P., 2017. Controls on iron mobilisation from volcanic ash at low pH: Insights from dissolution experiments and Mössbauer spectroscopy. Chem. Geol. 449, 73–81. https://doi.org/10.1016/J.CHEMGEO.2016.11.036

McCave, I.N., 1986. Local and global aspects of the bottom nepheloid layers in the world ocean. Netherlands J. Sea Res. 20, 167–181. https://doi.org/10.1016/0077-7579(86)90040-2

Moore, C.M., Mills, M.M., Arrigo, K.R., Berman-Frank, I., Bopp, L., Boyd, P.W., Galbraith, E.D., Geider, R.J., Guieu, C., Jaccard, S.L., Jickells, T.D., La Roche, J., Lenton, T.M., Mahowald, N.M., Marañón, E., Marinov, I., Moore, J.K., Nakatsuka, T., Oschlies, A., Saito, M.A., Thingstad, T.F., Tsuda, A., Ulloa, O., 2013. Processes and patterns of oceanic nutrient limitation. Nat. Geosci. 6, 701–710. https://doi.org/10.1038/ngeo1765

Morgan, J.L.L., Wasylenki, L.E., Nuester, J., Anbar, A.D., 2010. Fe Isotope Fractionation during Equilibration of Fe−Organic Complexes. Environ. Sci. Technol. 44, 6095–6101. https://doi.org/10.1021/ES100906Z

Murray, N.A., McManus, J., Palmer, M.R., Haley, B., Manners, H., 2018. Diagenesis in tephra-rich sediments from the Lesser Antilles Volcanic Arc: Pore fluid constraints. Geochim. Cosmochim. Acta 228, 119–135. https://doi.org/10.1016/J.GCA.2018.02.039

Murray, N.A., Muratli, J.M., Hartwell, A.M., Manners, H., Megowan, M.R., Goñi, M., Palmer, M., McManus, J., 2016. Data report: dissolved minor element compositions, sediment major and minor element concentrations, and reactive iron and manganese data from the Lesser Antilles volcanic arc region, IODP Expedition 340 Sites U1394, U1395, U1396, U1399, and U1400. Proc. Integr. Ocean Drill. Progr. 340. https://doi.org/10.2204/iodp.proc.340.207.2016

Oeser, M., Weyer, S., Horn, I., Schuth, S., 2014. High-Precision Fe and Mg Isotope Ratios of Silicate Reference Glasses Determined In Situ by Femtosecond LA-MC-ICP-MS and by Solution Nebulisation MC-ICP-MS. Geostand. Geoanalytical Res. 38, 311–328. https://doi.org/10.1111/J.1751-908X.2014.00288.X

Olgun, N., Duggen, S., Croot, P.L., Delmelle, P., Dietze, H., Schacht, U., Óskarsson, N., Siebe, C., Auer, A., Garbe-Schönberg, D., 2011. Surface ocean iron fertilization: The role of airborne volcanic ash from subduction zone and hot spot volcanoes and related iron fluxes into the Pacific Ocean. Global Biogeochem. Cycles 25, n/a-n/a. https://doi.org/10.1029/2009GB003761

Olgun, N., Duggen, S., Langmann, B., Hort, M., Waythomas, C., Hoffmann, L., Croot, P., 2013. Geochemical evidence of oceanic iron fertilization by the Kasatochi volcanic eruption in 2008 and the potential impacts on Pacific sockeye salmon. Mar. Ecol. Prog. Ser. 488, 81–88. https://doi.org/10.3354/meps10403

Palmer, M.R., Hatter, S.J., Gernon, T.M., Taylor, R.N., Cassidy, M., Johnson, P., Le Friant, A., Ishizuka, O., 2016. Discovery of a large 2.4 Ma Plinian eruption of Basse-Terre, Guadeloupe, from the marine sediment record. Geology 44, 123–126. https://doi.org/10.1130/G37193.1

Peters, J.L., Murray, R.W., Sparks, J.W., Coleman, D.S., Leckie, R.M., Sigurdsson, H., Acton, G.D., Abrams, L.J., Bralower, T.J., Carey, S.N., Chaisson, W.P., Cotillon, P., Cunningham, A.D., D'Hondt, S.L., Droxler, A.W., Galbrun, B., Gonzalez, J., Haug, G.H., Kameo, K., King, J.W.,

Lind, I.L., Louvel, V., Lyons, T.W., Mutti, M., Myers, G., Pearce, R.B., Pearson, D.G., Peterson, L.C., Roehl, U., 2000. Terrigenous matter and dispersed ash in sediment from the Caribbean Sea; results from Leg 165. Proc. Ocean Drill. Program, Sci. Results 165, 115–124. https://doi.org/10.2973/odp.proc.sr.165.003.2000

Pisias, N.G., Murray, R.W., Scudder, R.P., 2013. Multivariate statistical analysis and partitioning of sedimentary geochemical data sets: General principles and specific MATLAB scripts. Geochemistry, Geophys. Geosystems 14, 4015–4020. https://doi.org/10.1002/ggge.20247

Pyle, D.M., 1995. Mass and energy budgets of explosive volcanic eruptions. Geophys. Res. Lett. 22, 563–566. https://doi.org/10.1029/95GL00052

Radic, A., Lacan, F., Murray, J.W., 2011. Iron isotopes in the seawater of the equatorial Pacific Ocean: New constraints for the oceanic iron cycle. Earth Planet. Sci. Lett. 306, 1–10. https://doi.org/10.1016/j.epsl.2011.03.015

Reid, R.P., Carey, S.N., Ross, D.R., 1996. Late Quaternary sedimentation in the Lesser Antilles island arc. Bull. Geol. Soc. Am. 108, 78–100. https://doi.org/10.1130/0016-7606(1996)108<0078:LQSITL>2.3.CO;2

Rudnick, R.L., Gao, S., 2013. Composition of the Continental Crust. Treatise Geochemistry Second Ed. 4, 1–51. https://doi.org/10.1016/B978-0-08-095975-7.00301-6

Schindlbeck, J.C., Kutterolf, S., Freundt, A., Alvarado, G.E., Wang, K. -L., Straub, S.M., Hemming, S.R., Frische, M., Woodhead, J.D., 2016. Late Cenozoic tephrostratigraphy offshore the southern Central American Volcanic Arc: 1. Tephra ages and provenance. Geochemistry, Geophys. Geosystems 17, 4641–4668. https://doi.org/10.1002/2016GC006503@10.1002/(ISSN)1525-2027.SUBDUCT2

Schindlbeck, J.C., Kutterolf, S., Freundt, A., Eisele, S., Wang, K.-L., Frische, M., 2018. Miocene to Holocene Marine Tephrostratigraphy Offshore Northern Central America and Southern Mexico: Pulsed Activity of Known Volcanic Complexes. Geochemistry, Geophys. Geosystems 19, 4143–4173. https://doi.org/10.1029/2018GC007832

Schoenberg, R., Von Blanckenburg, F., 2005. An assessment of the accuracy of stable Fe isotope ratio measurements on samples with organic and inorganic matrices by high-resolution multicollector ICP-MS. Int. J. Mass Spectrom. 242, 257–272. https://doi.org/10.1016/J.IJMS.2004.11.025

Scudder, R.P., Murray, R.W., Plank, T., 2009. Dispersed ash in deeply buried sediment from the northwest Pacific Ocean: An example from the Izu–Bonin arc (ODP Site 1149). Earth Planet. Sci. Lett. 284, 639–648. https://doi.org/10.1016/J.EPSL.2009.05.037

Scudder, R.P., Murray, R.W., Schindlbeck, J.C., Kutterolf, S., Hauff, F., McKinley, C.C., 2014. Regional-scale input of dispersed and discrete volcanic ash to the Izu-Bonin and Mariana subduction zones. Geochemistry, Geophys. Geosystems 15, 4369–4379. https://doi.org/10.1002/2014GC005561

Scudder, R.P., Murray, R.W., Schindlbeck, J.C., Kutterolf, S., Hauff, F., Underwood, M.B., Gwizd, S., Lauzon, R., McKinley, C.C., 2016. Geochemical approaches to the quantification of dispersed volcanic ash in marine sediment. Prog. Earth Planet. Sci. 3, 1. https://doi.org/10.1186/s40645-015-0077-y

Simonella, L.E., Palomeque, M.E., Croot, P.L., Stein, A., Kupczewski, M., Rosales, A., Montes, M.L., Colombo, F., García, M.G., Villarosa, G., Gaiero, D.M., 2015. Soluble iron inputs to the Southern Ocean through recent andesitic to rhyolitic volcanic ash eruptions from the Patagonian Andes. Global Biogeochem. Cycles 29, 1125–1144. https://doi.org/10.1002/2015GB005177

Tagliabue, A., Aumont, O., Death, R., Dunne, J.P., Dutkiewicz, S., Galbraith, E., Misumi, K., Moore, J.K., Ridgwell, A., Sherman, E., Stock, C., Vichi, M., Völker, C., Yool, A., 2016. How well do

global ocean biogeochemistry models simulate dissolved iron distributions? Global Biogeochem. Cycles 30, 149–174. https://doi.org/10.1002/2015GB005289

Tagliabue, A., Bowie, A.R., Boyd, P.W., Buck, K.N., Johnson, K.S., Saito, M.A., 2017. The integral role of iron in ocean biogeochemistry. Nature. https://doi.org/10.1038/nature21058

Weyer, S., Schwieters, J.B., 2003. High precision Fe isotope measurements with high mass resolution MC-ICPMS. Int. J. Mass Spectrom. 226, 355–368. https://doi.org/10.1016/S1387-3806(03)00078-2

Figures

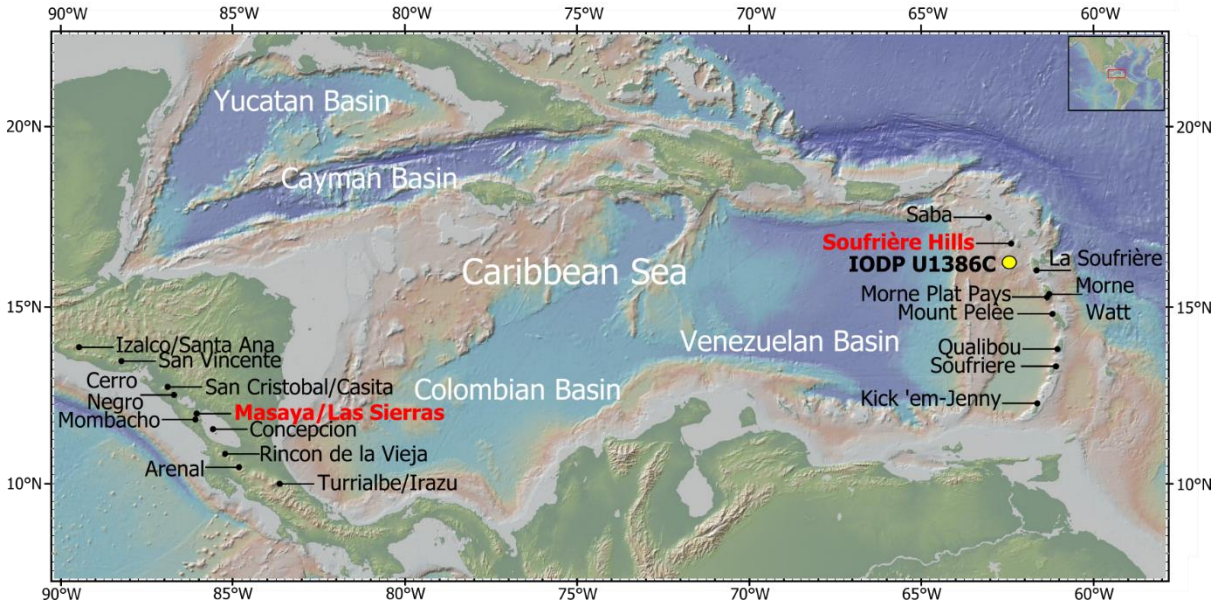

Figure 1: Map indicating location of Hole U1396C (yellow circle) within the Caribbean Sea area. Also shown are the locations of the primary recently active volcanoes in the region. The location of Las Sierras, and Soufrière Hills volcanoes, used in the modelling here, are indicated by bold red text. Map created in ArcMap 10.3, Environmental Systems Resource Institute, ArcMap 10.3 ESRI, Redlands, California, http://desktop.arcgis.com/en/arcmap/.

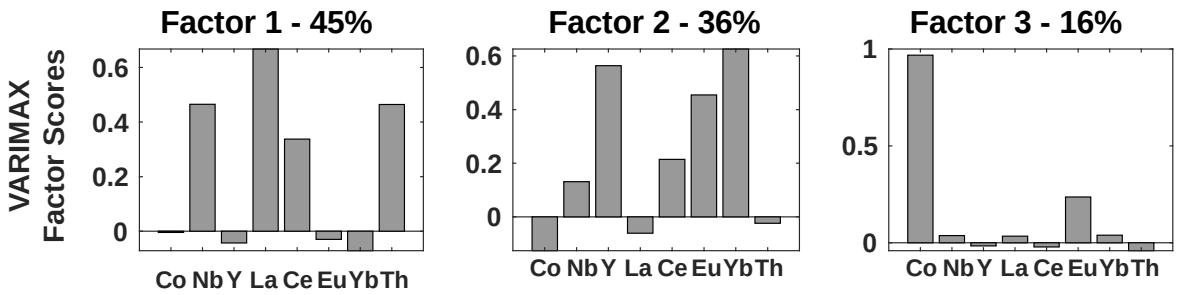

Figure 2: The VARIMAX factor scores from the Q-mode factor analysis. Elements affiliated with the aluminosilicate fraction produced three factors that explain 97% of the variability of the dataset (45%, 36%, and 16%, respectively).

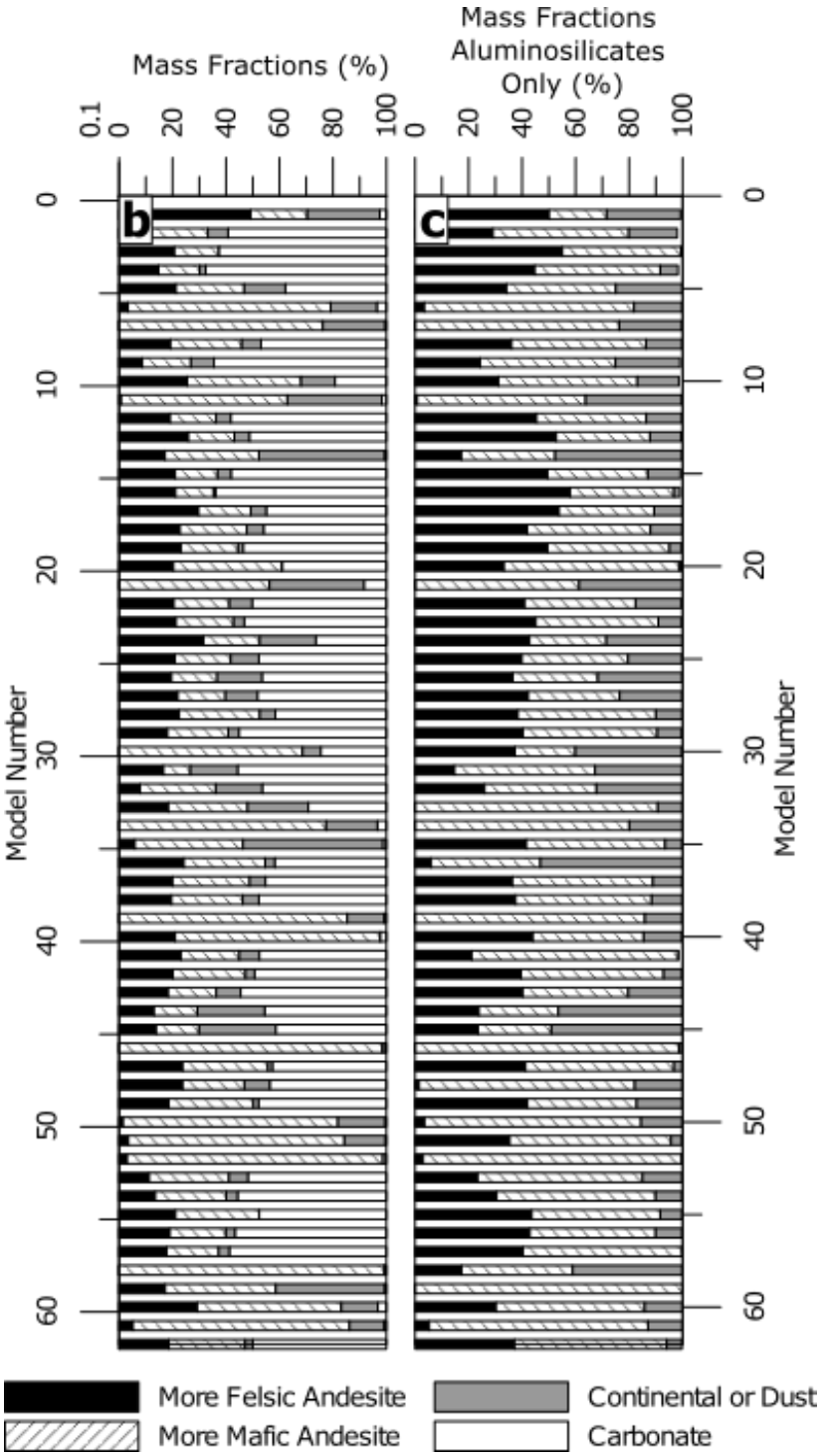

Figure 3: a) The results of the CLS model. Modelled end-member mass fractions in each discrete layer or bulk sediment sample plotted with the same scale as panel a. Black and hashed white indicate the

mass fractions of the more felsic and more mafic andesites, respectively. Grey represents contributions from an upper continental crust or dust source. The remaining white area represents the carbonate fraction of bulk sediment. b) The CLS modelled mass fractions of only the aluminosilicate fraction of the samples (excluding the carbonate fraction).

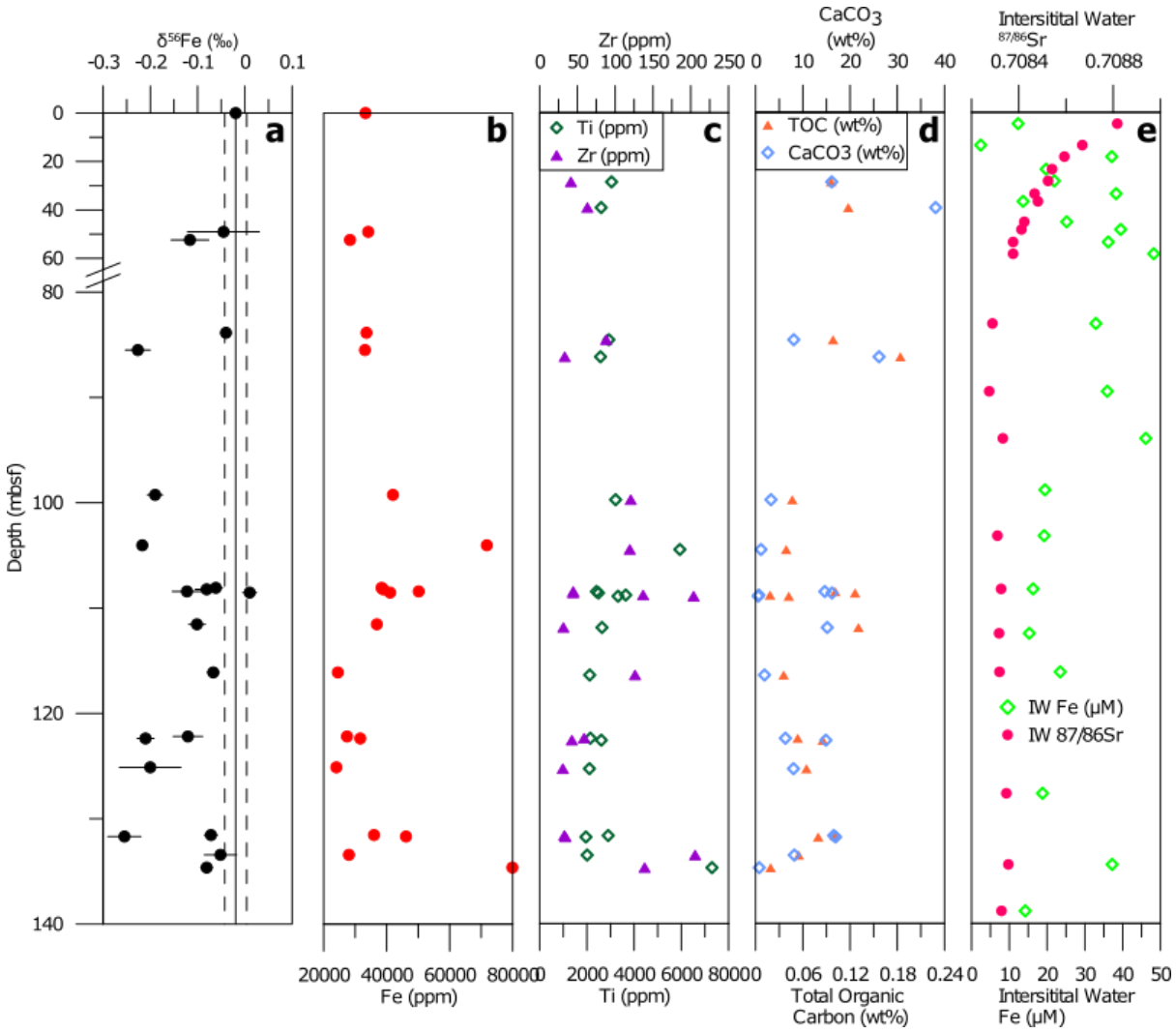

Figure 4: Geochemical parameters from U1396C. (a) Fe isotope composition of analysed samples, with error bars indicating measurement error (2SD). The measured value of terrestrially emplaced ash from Montserrat indicated with a black line, with measurement error indicated by dashed lines. (b) Fe content of samples analysed for isotopic composition. (c) Ti and Zr content for the same samples. (d) calcium carbonate and organic carbon (total carbon) content for the same samples. (e) Interstitial water Fe content and Sr isotope composition (from Murray et al., 2018).

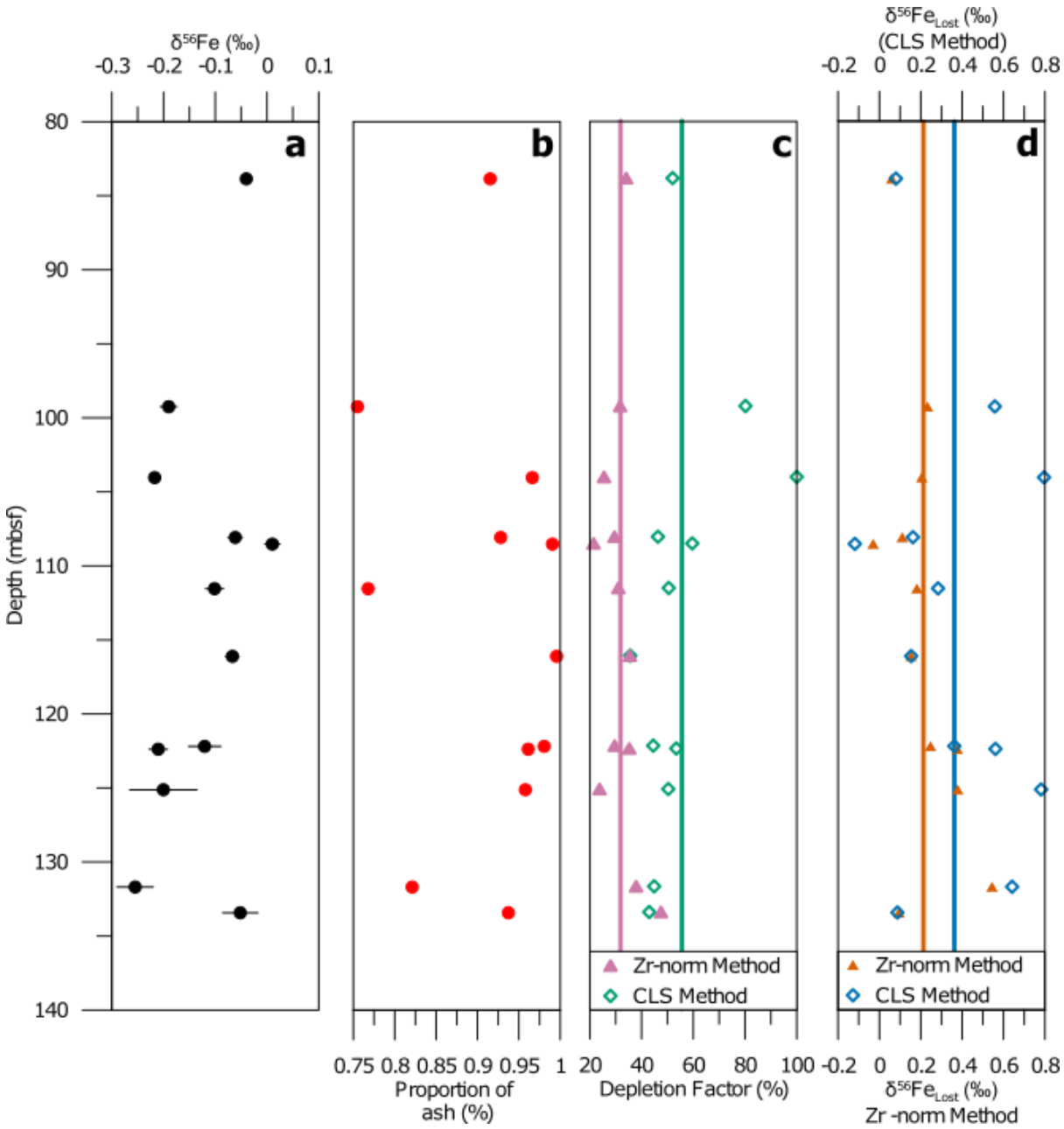

Figure 5: Parameters used in the mass balance modelling of the lost Fe fraction ($\delta^{56}Fe_{Lost}$), or the isotopic composition of Fe flux from samples with >75% tephra. (a) Bulk $\delta^{56}Fe$ measurements for the samples with high enough ash content to be modelled (>75%). (b) The proportion of ash in each sample, as calculated from the multivariate modelling. (c) Fe depletion factor (DF) calculations, DF Method 1 from Lee et al. (2018) and DF Method 2 from our multivariate partitioning. Individual models are

indicated with coloured symbols, and the mean of each method is highlighted with a coloured line. (d) The calculated $\delta^{56}Fe_{Lost}$ for each of the samples, with the calculations made using the depletion factors displayed in panel c. Again, the mean of the outputs is highlighted with a coloured line.